INSTITUTE OF PHYSICS PUBLISHING SEMICONDUCTOR SCIENCE AND TECHNOLOGY

Semicond. Sci. Technol. **17** (2002) 947–951 PII: S0268-1242(02)36599-4

Optical and transport properties of short-period InAs/GaAs superlattices near quantum dot formation

V A Kulbachinskii[1], R A Lunin[1], V A Rogozin[1], V G Mokerov[2], Yu V Fedorov[2], Yu V Khabarov[2] and A de Visser[3]

[1] Low Temperature Physics Department, Moscow State University, 119899, Moscow, Russia
[2] Institute of Radioengineering and Electronics, Russian Academy of Sciences, 103907 Moscow, Russia
[3] Van der Waals–Zeeman Institute, University of Amsterdam, Valckenierstraat 65, 1018 XE Amsterdam, The Netherlands

E-mail: devisser@science.uva.nl

Received 2 May 2002
Published 22 July 2002
Online at stacks.iop.org/SST/17/947

Abstract
We have investigated the optical and transport properties of short-period superlattices of InAs/GaAs, grown by molecular beam epitaxy, with different numbers of periods ($3 \leqslant N \leqslant 24$) and a total thickness of 14 nm. Band structure calculations show that these superlattices represent a quantum well with average composition $In_{0.16}Ga_{0.84}As$. The electron wavefunctions are only slightly modulated by the superlattice potential as compared to a single quantum well with the same composition, which was grown as a reference sample. The photoluminescence, the resistance, the Shubnikov–de Haas effect and the Hall effect have been measured as a function of the InAs layer thickness Q in the range of $0.33 \leqslant Q \leqslant 2.7$ monolayers (ML). The electron densities range from 6.8 to 11.5 $\times 10^{11}$ cm^{-2} for $Q \leqslant 2.0$ ML. The photoluminescence and magneto-transport data show that only one sub-band is occupied. When $Q \geqslant 2.7$ ML, quantum dots are formed and the metallic type of conductivity changes to variable range hopping conductivity.

1. Introduction

In recent years, much research has been focused on self-organized ensembles of quantum dots. Such quantum dots are quasi-zero-dimensional objects (with sizes of ~5–20 nm), which form during hetero-epitaxial growth due to the mismatch of the lattice parameters of the grown material and the substrate. The mechanism of nucleation and the formation of quantum dots in the Stransky–Krastanov growth mode have been studied intensively [1–6]. The process of self-organized growth of InAs quantum dots on the surface of GaAs starts when the thickness Q of the InAs layer exceeds some critical value. There is a large amount of literature dealing with the investigation of the optical properties of undoped structures in the quantum dot regime [3, 6]. However, structures with InAs layer thicknesses below the threshold for quantum dot formation have been studied less. Here, we report on the optical and electrical properties of doped structures at the initial stage of quantum dot formation. Short-period InAs/GaAs superlattices with periods of $3 \leqslant N \leqslant 24$ and a total thickness of 14 nm were prepared with very thin InAs layers ranging from 0.33 to 2.7 monolayers (ML). Energy band calculations show that the wavefunctions of the superlattice are equivalent to those of a single quantum well, with a small modulation due to the periodic potential of the superlattice. In order to investigate the optical and electrical properties of these superlattices we measured the photoluminescence (PL) at a temperature $T = 77$ K and the resistance R in the T range 1–300 K. In addition, Shubnikov–de Haas (SdH) and Hall effect measurements were carried out in a long-pulse (1 s) high-field magnet at the University of Amsterdam. The maximum field was 40 T and the T range was 1.4–4.2 K.

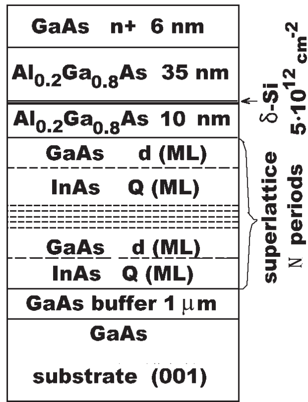

Figure 1. Schematic diagram of the short-period InAs/GaAs superlattice structures. The number of periods is $3 \leqslant N \leqslant 24$. The InAs layer has a thickness Q and the GaAs layer has a thickness d. The total width of the superlattice is 14 nm.

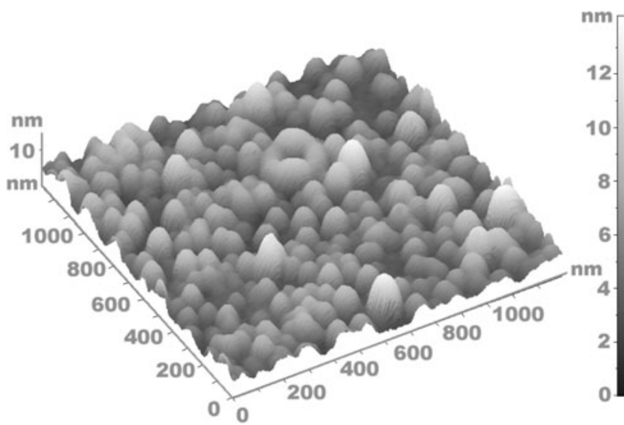

Figure 2. AFM image of sample 8 ($Q = 2.7$ ML) after selective etching of the cap layer. Quantum dots are formed.

2. Samples

The short-period superlattice structures were grown by molecular beam epitaxy (MBE) at a temperature of 490 °C on semi-insulating (001) GaAs substrates. A schematic diagram of the structure is given in figure 1. The N period InAs/GaAs superlattices, with a total thickness of 14 nm, were grown on a 1 μm thick GaAs buffer layer. The value of 14 nm of the total thickness is dictated by the optimal composition $In_{0.16}Ga_{0.84}As$ from the point of view of the quality of the crystal structure. Larger thicknesses in strained structures with the same composition may give rise to lattice defects. The effective thickness Q of the InAs layers ranged from 0.33 to 2.7 ML, while the thickness d of the GaAs layers in the superlattice was varied correspondingly from 1.7 to 13.5 ML, so as to keep the mean composition of the superlattice equivalent to that of the solid solution $In_{0.16}Ga_{0.84}As$. The Si δ-doping layer, with a Si sheet concentration 5×10^{12} cm^{-2}, was separated from the superlattice by a 10 nm thick spacer layer of composition $Al_{0.2}Ga_{0.8}As$. Subsequently, a 35 nm thick layer of $Al_{0.2}Ga_{0.8}As$ was grown, followed by a 6 nm thick GaAs cap layer. As a reference sample, a single quantum well $In_{0.16}Ga_{0.84}As$ (well width 14 nm) was grown.

In order to measure in-plane electron transport, Hall bars were prepared from the wafers for all structures. The (double) Hall bars were L-shaped to allow the current I to flow parallel (‖) and perpendicular (⊥) to the [110] direction in the same sample. This allows for an accurate investigation of anisotropy in the transport properties. The relevant parameters of the structures are listed in table 1. Photoluminescence and atomic force microscopy (AFM) data clearly demonstrate that for $Q < 2.7$ ML nanoscale semiconductor islands of InAs are formed, while for $Q \geqslant 2.7$ ML InAs quantum dots form. The latter is illustrated in figure 2, which shows the AFM image of sample 8 ($Q = 2.7$ ML) after selective etching of the surface.

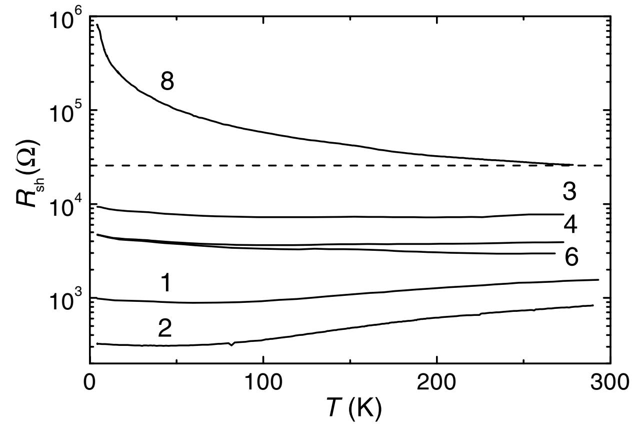

Figure 3. Temperature dependence of the sheet resistance for samples 1–4, 6 and 8. The dashed line corresponds to the critical value of the resistivity h/e^2.

3. Results and discussion

3.1. Temperature dependence of the resistivity

The temperature dependence of the sheet resistivity $R_{sh}(T)$ of some selected structures is shown in figure 3. For the samples with $Q \leqslant 2.0$ ML, the resistivity has a very weak temperature dependence with an absolute value of the sheet conductivity more than e^2/h, i.e. the critical conductivity value for the transition from the two-dimensional (2D) metallic phase to the insulating phase. At low temperatures the conductivity shows a logarithmic temperature dependence, $\sigma_{sh} \sim \ln T$, which is characteristic of weak localization [7]. The $\ln T$ behaviour is typically valid in the range $2 < T < 15$ K, as illustrated for samples 2 and 4 in figure 4. At lower T the conductivity starts to saturate. The reason for this saturation is not clear.

The resistivity of the structure with $Q = 2.7$ ML (sample 8) behaves very differently. $R_{sh}(T) \sim h/e^2$ at room temperature and increases with decreasing temperature. This is in line with the formation of quantum dots in the layers. At the lowest temperatures the resistivity enters the variable range hopping conductivity regime for the 2D case, $R_{sh}(T) \sim \exp[(T_0/T)^{1/3}]$ [8], as shown in the inset in figure 4.

3.2. Photoluminescence

Figure 5 shows the PL spectra for the different structures. For samples with $Q \leqslant 2.0$ ML, two peaks are observed: (i) a low-energy peak with a maximum at photon energies 1.356–1.375 eV; (ii) a high-energy peak with a maximum at photon

Table 1. Structural and electronic parameters of short-period InAs/GaAs superlattices with a total thickness of 14 nm. Q and d are the InAs and GaAs layer thicknesses expressed in ML, respectively. N is the number of superlattice periods. Maxima in the PL spectra are observed at $h\nu_{max}$ (at $T = 77$ K). n is the carrier density determined by the Hall effect and μ is the mobility (at $T = 4.2$ K).

Sample number	Q (InAs, ML)	D (GaAs, ML)	Number of periods N	$h\nu_{max}$ (eV)	n (10^{11} cm^{-2})	μ (cm^2 V^{-1} s^{-1})
1	Quantum well $In_{0.16}Ga_{0.84}As$	Quantum well $In_{0.16}Ga_{0.84}As$	–	1.434, 1.375	8.1	8100
2	0.33	1.7	24	1.419, 1.367	11.5	9400
3	0.67	3.4	12	1.411, 1.369	7.2	2060
4	1.00	5.0	8	1.411, 1.370	7.3	2450
5	1.33	6.7	6	1.418, 1.374	8.7	4220
6	1.58	8.0	5	1.404, 1.368	6.8	4910
7	2.00	10.0	4	1.406, 1.356	10.4	7060
8	2.70	13.5	3	1.390, 1.265	1.5	50

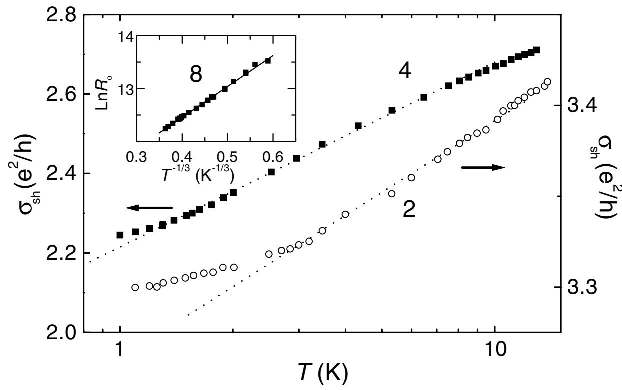

Figure 4. Temperature dependence of the sheet conductivity (in units of e^2/h) for samples 2 and 4. The data follow an $\ln T$ dependence between ~2–15 K. The inset shows the low-temperature conductivity for sample 8 (with quantum dots). The data follow the Mott law for variable range hopping conductivity: $R_{sh} \sim \exp(T_0/T)^{1/3}$ (solid line).

energies 1.406–1.434 eV (see also table 1). These two peaks correspond to optical transitions from the two electronic sub-bands, i.e. from the occupied lower sub-band and the unoccupied upper sub-band (see section 3.4), to the hole sub-band [9]. The intensity of the low-energy peak is always higher. This is similar to the case of undoped quantum wells, where the optical transition from the lowest sub-band is readily observed in PL spectra, while the transition from the upper sub-band is very weak. A distinctly different behaviour is observed when the effective thickness of the InAs layers $Q \geqslant 2.7$ ML. A new broad and intense PL peak with a maximum at 1.265 eV appears in the long-wavelength region of the PL spectrum (see data for sample 8 in figure 5). As shown in [1–3], such a transformation of the PL spectrum can be attributed to the change from 2D layer-by-layer growth to the formation of vertically-stacked quantum dots. The presence of quantum dots in sample 8 was confirmed by AFM (see figure 2).

A second noteworthy feature of the PL spectra is the non-monotonic dependence of the intensity I_{PL} on the InAs layer thickness Q. The largest intensities are observed for sample 2 ($Q = 0.33$ ML) and sample 7 ($Q = 2.0$ ML). For the same samples, we observe maxima of the electron mobility μ (see table 1).

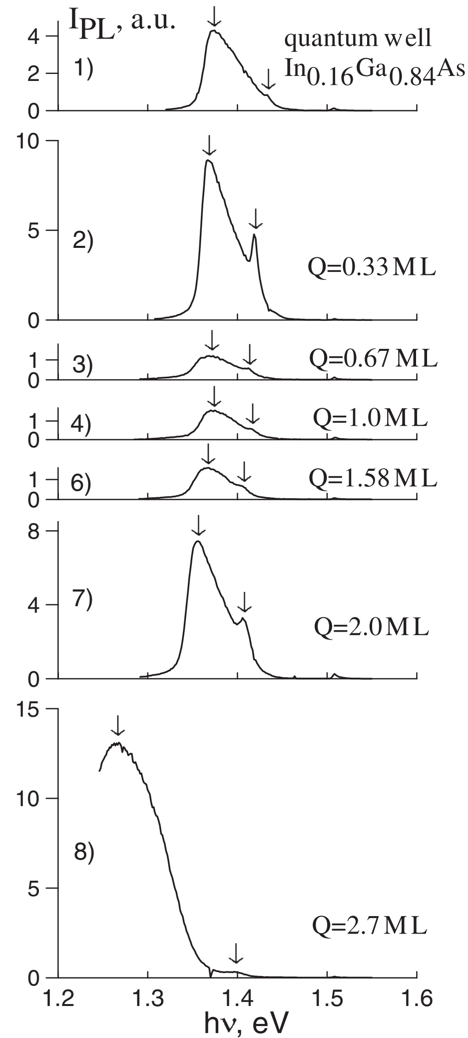

Figure 5. PL spectra of short-period InAs/GaAs superlattices with InAs layer thickness 0.33 ML $\leqslant Q \leqslant$ 2.7 ML. For comparison, the spectrum for a single quantum well with composition $In_{0.16}Ga_{0.84}As$ (sample 1) is also shown. The arrows indicate the positions of maxima.

3.3. The energy spectrum

For all structures, the electron wavefunctions $\psi_i(z)$ and the energies E_i were determined in the effective mass approximation by the self-consistent solution of the

one-dimensional Schrödinger and Poisson equations [10,11]. In the Schrödinger equation

$$\left[-\frac{\hbar^2}{2}\frac{\mathrm{d}}{\mathrm{d}z}\left(\frac{1}{m^*(z)}\frac{\mathrm{d}}{\mathrm{d}z}\right)+U(z)\right]\psi_i(z)=E_i\psi_i(z) \qquad (1)$$

the potential energy $U(z) = U_c(z) + U_H(z) + U_{xc}(z)$ is the sum of the conduction-band discontinuity $U_c(z)$ at the heterojunctions, the electrostatic potential energy $U_H(z)$ (Hartree potential) and the exchange-correlation potential $U_{xc}(z)$. The electrostatic potential energy is determined by the Poisson equation

$$\frac{\mathrm{d}}{\mathrm{d}z}\left(\varepsilon_0\varepsilon(z)\frac{\mathrm{d}U_H(z)}{\mathrm{d}z}\right)=e^2[N(z)-n(z)] \qquad (2)$$

where ε_0 is the permittivity of the vacuum, ε is the permittivity of the material, $N(z)$ is the three-dimensional (3D) density of ionized donors and

$$n(z)=\frac{m^*}{\pi\hbar^2}\sum_i[E_F-E_i]\theta[E_F-E_i]|\psi_i(z)|^2 \qquad (3)$$

is the electron concentration at $T = 0$ K, with $\theta\ (x)$ being the Heaviside function. The exchange-correlation potential was approximated by the formula [12]

$$U_{xc}=-\left[1+0.0545r_S\ln\left(1+\frac{11.4}{r_S}\right)\right]\frac{2}{\pi\alpha r_S}Ry^* \qquad (4)$$

where

$$\alpha=\left(\frac{4}{9\pi}\right)^{1/3},\qquad r_S=\left(\frac{4\pi a_B^3 n(z)}{3}\right)^{-1/3},$$
$$a_B^*=\frac{4\pi\varepsilon_0\varepsilon\hbar^2}{m^*e^2},\qquad Ry^*=\frac{e^2}{8\pi\varepsilon_0\varepsilon a_B^*}. \qquad (5)$$

The values of the conduction-band and valence-band discontinuities of GaAs and strained InAs were taken to be equal to $\Delta U_c = 0.535$ eV and $\Delta U_v = 0.385$ eV [13], respectively. The electron effective mass in strained InAs is equal to $m_e^{st} = 0.0365\ m_0$ [14].

Using the calculated profile of the conduction band, we determined the profile of the valence band and the hole energy levels in the quantum well. Typical examples of the profile of the bottom of the conduction band E_c, the position of the two sub-bands E_0 and E_1, and the corresponding wavefunctions are shown in figure 6 for samples 4 and 7. The energy is measured with respect to the Fermi level E_F. In all samples, only the lowest energy level is occupied by electrons. This is confirmed by the SdH data (see section 3.4). The calculated energies of the optical transitions are in good agreement with the positions of the peaks in the PL spectra. Figure 6 shows that the wavefunctions of the superlattices are almost identical to those of a single quantum well with the average composition $In_{0.16}Ga_{0.84}As$ and the same well width. The difference is a weak modulation due to the superlattice potential. We conclude that a very-short-period superlattice behaves like a single quantum well with a weak modulation of the potential.

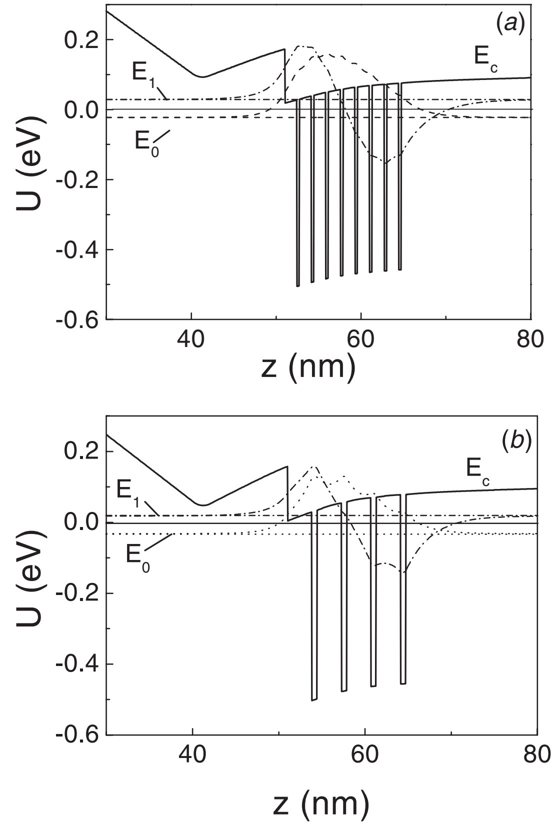

Figure 6. Calculated band diagram for superlattice structures: (*a*) sample 7 with eight periods; (*b*) sample 4 with four periods. E_c denotes the bottom of the conduction band. The lowest two sub-bands E_0 (dashed line) and E_1 (dash–dotted line) are indicated together with the corresponding wavefunctions. The Fermi level is represented by the solid line.

3.4. Magnetoresistance

For all samples we observed a negative magnetoresistance at low temperatures in low magnetic fields ($B < 0.1$ T). Such a dependence is expected for the weak localization regime in the 2D case [7], which was inferred from the logarithmic decrease of the conductivity with decreasing temperature (see figure 4).

Figure 7 shows high-field transport data for samples 4 and 6. The longitudinal resistance shows SdH oscillations, while the quantum Hall effect is observed for fields exceeding ~7 T. The transversal resistance R_{xy} shows clear plateau values at the integer filling fraction $\nu = 1$, 2 and 3. The fast Fourier transform (FFT) of the SdH signal in the low magnetic field data ($B \lesssim 8$ T, see inset of figure 7) shows one single frequency, which implies that only the lowest sub-band is occupied. The carrier concentrations determined from the period of the SdH effect coincide with those determined from the low-field Hall effect and fall in the range $n = 1.5$–12×10^{11} cm^{-2} for the different structures at $T = 4.2$ K.

The Hall mobilities μ for the different structures with $Q \leqslant 2$ ML range from 0.21 to 0.94 m^2 V^{-1} s^{-1} at $T =$ 4.2 K. The highest mobility values, $\mu = 0.94$ m^2 V^{-1} s^{-1} and $\mu = 0.71$ cm^2 V^{-1} s^{-1}, are observed for samples 2 and 7, respectively. These relatively high mobilities are possibly explained by the weakness of the elastic strain fluctuations and a near-perfect crystal lattice as compared to the solid solution $In_{0.16}Ga_{0.84}As$. It is worth noting that, for these two samples, the intensity of the PL peak is much higher also. In sample 8, quantum dots are formed and the electron concentration is reduced to $n = 1.5 \times 10^{11}$ cm^{-2}, i.e. much smaller than

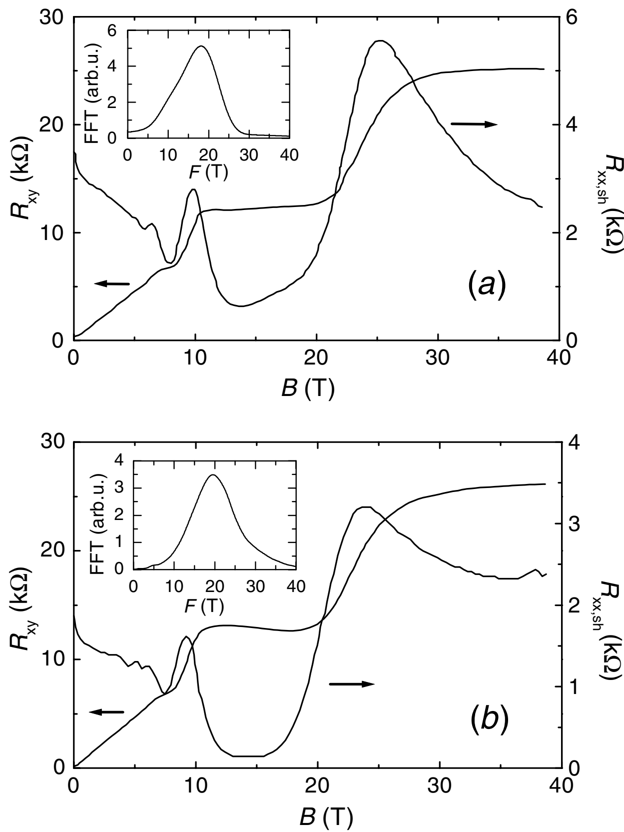

Figure 7. High-field magneto-transport data for (*a*) sample 4 with $Q = 1.0$ ML and (*b*) sample 6 with $Q = 1.58$ ML, taken at $T = 4.2$ K. $R_{xx,\mathrm{sh}}$ is the longitudinal sheet resistance and R_{xy} is the transversal resistance. The quantum Hall effect becomes visible above fields of ∼8 T. The insets show the FFT of the SdH signal.

in the other structures. Consequently, the electron mobility $\mu = 0.005$ $\mathrm{m^2\ V^{-1}\ s^{-1}}$ is very low.

3.5. Anisotropy of conductivity

For all superlattice samples, the transport experiments on the L-shaped Hall bars signal a significant anisotropy of the resistivity. Anisotropy was not detected in the transport measurements on the quantum well with composition $In_{0.16}Ga_{0.84}As$ (sample 1). The ratio of the resistance $R_\perp/R_\parallel$ depends on the thickness Q and attains a value up to ∼1.3. The corresponding anisotropic electron mobility is related to an asymmetric dislocation distribution [15]. The anisotropy of the resistance in 2D electron systems is typical for structures with preferential growth of deposited material in one direction (see, e.g. [16, 17]). The observed Q dependence of the anisotropy indicates that elongated island growth sets in above a certain threshold value [18].

4. Conclusions and summary

The optical and transport properties of MBE-grown short-period superlattices of InAs/GaAs with different numbers of periods ($3 \leqslant N \leqslant 24$) have been studied. The total thickness of the superlattice is 14 nm, which was kept constant by varying the thickness Q of the InAs layer and d of the GaAs layer. The electronic wavefunctions were calculated self-consistently by solving the one-dimensional Schrödinger and Poisson equations. For $Q \leqslant 2.0$ ML, our superlattices can be described as a single quantum well of average composition $In_{0.16}Ga_{0.84}As$, with electronic wavefunctions slightly modulated due to the superlattice potential. The PL and the high-field SdH effect show that only the lowest subband is occupied. For some of the structures, we observe the quantum Hall effect. For $Q > 2.0$ ML, the PL and the variable range hopping conductivity resistivity data provide further evidence for the formation of quantum dots. The PL peak and the electron density and mobility do not depend monotonically on the InAs layer thickness. For $Q = 0.33$ ML and $Q = 2.0$ ML, enhanced values for the intensity of the PL peak and mobility are observed. This is possibly because of the higher quality of these structures, due to a more effective relaxation of the strain. A small but significant anisotropy in the resistance was observed which depends on the thickness of the InAs layers, as expected for elongated island growth.

Acknowledgments

This work was supported by the RFBR under grants nos 00-02-17493 and 01-02-17748.

References

[1] Ledentsov N N, Ustinov V M, Shchukin V A, Kop'ev P S, Alferov J I and Bimberg D 1998 *Semiconductors* **32** 343
[2] Bimberg D, Shchukin V A, Ledentsov N N and Krost A 1998 *Appl. Surf. Sci.* **130–132** 713
[3] Bimberg D, Grundman M and Ledentsov N N 1998 *Quantum Dot Heterostructures* (New York: Wiley)
[4] Kulbachinskii V A, Kytin V G, Lunin R A, Golikov A V, Malkina I G, Zvonkov B N and Safyanov Yu N 1999 *Semiconductors* **33** 318
[5] Fry P W *et al* 2000 *Phys. Rev. Lett.* **84** 733
[6] Yoffe A D 2001 *Adv. Phys.* **50** 1
[7] Altshuler B L and Aronov A G 1985 *Modern Problems in Condensed Matter Sciences* vol 10 ed A L Efros and M Pollak (Amsterdam: North-Holland)
[8] Shklovskii B I and Efros A L 1984 *Electronic Properties of Doped Semiconductors* (Berlin: Springer)
[9] Yuan Y K, Mohammed K, Pudensi M A A and Mezz J L 1984 *Appl. Phys. Lett.* **45** 739
[10] Ando T 1982 *J. Phys. Soc. Jpn.* **51** 3893
[11] Kulbachinskii V A, Lunin R A, Kytin V G, Bugaev A S and Senichkin A S 1996 *JETP* **83** 841
[12] Gunnarsson O and Lundqvist B I 1976 *Phys. Rev.* B **13** 4274
[13] Brübach J, Silov A Yu, Haverkort J E M, v.d.Vleuten W and Wolter J H 1999 *Phys. Rev.* B **59** 10315
[14] Foulon Y and Priester C 1991 *Phys. Rev.* B **44** 5889
[15] Schweizer T, Kohler K, Rothemund W and Ganser P 1991 *Appl. Phys. Lett.* **59** 2736
[16] De Visser A, Kadushkin V I, Kulbachinskii V A, Kytin V G, Senichkin A P and Shangina E L 1994 *JETP Lett.* **59** 363
[17] Kulbachinskii V A, Kytin V G, Kadushkin V I and Senichkin A P 1995 *Solid State Phys.* **37** 2693
[18] Horikoshi Y 1994 *Handbook of Crystal Growth 3, Part B: Growth Mechanisms and Dynamics* ed D T J Hurle (Amsterdam: Elsevier)